Journal of MATERIALS RESEARCH

Invited Feature Paper
DOI: 10.1557/jmr.2020.114

Compressive failure of hydrogel spheres

Jeremiah D. James[1], Jacob M. Ludwick[1], Mackenzie L. Wheeler[1], Michelle L. Oyen[1,a)]
[1]Department of Engineering, East Carolina University, Greenville, North Carolina 27858, USA
[a)]Address all correspondence to this author. e-mail: oyenm18@ecu.edu
This paper has been selected as an Invited Feature Paper.
Received: 14 February 2020; accepted: 20 April 2020

Hydrogels have gained recent attention for biomedical applications because of their large water content, which imparts biocompatibility. However, their mechanical properties can be limiting. There has been significant recent interest in the strength and fracture toughness of hydrogel materials in addition to their stiffness and time-dependent behavior. Hydrogels can fail in a brittle manner, although they are extremely compliant. In this work, the failure and fracture of hydrogels are examined using a compression test of spherical hydrogel particles. Spheres of commercially available polyacrylamide–potassium polyacrylate were hydrated and tested to failure in compression as a function of loading rate. The spheres exhibited little relaxation when compressed to small fixed displacements. The distributions of strength values obtained were examined in a particle fracture framework previously used for brittle ceramics. There was loading rate dependence apparent in the measured peak force and calculated peak strength values, but the data fell on a single empirical distribution function of strength for the hydrogels regardless of loading rate. Strength values for these hydrogels were mostly in the range of 0.05–0.3 MPa, illustrating the challenges using hydrogels for mechanically demanding applications such as tissue engineering.

Introduction

There has been considerable recent interest in hydrogel materials—hydrated polymer networks with very large water contents—for biomedical applications including tissue engineering [1, 2] and drug delivery [3, 4]. The large water contents of these materials allow for excellent biocompatibility, and the polymer networks can be constructed from a range of natural and synthetic polymeric base chemistries [5]. Furthermore, the polymer networks can be chemically or physically cross-linked [6], and composite gels with double independent networks [7, 8], nanoparticles [9], or nanofibers [10, 11] can be easily constructed. Overall, this very large parameter space of chemistries gives rise to an interesting class of materials with fascinating structure–property relationships.

Because of the large water contents inherent to these hydrogel materials, the mechanical properties have been one key limitation in their biomedical use [6], especially for physically demanding tissue engineering applications, such as articular cartilage [12, 13] or cornea [14]. There has been particular recent interest in failure and fracture properties of single network hydrogels [15], double network hydrogels [7], and nanofiber-reinforced hydrogel composites [16]. Comparisons of physical properties of soft biological tissues have shown that both strength (1–10 MPa) and fracture resistance (1–10 kJ/m^2) of soft tissues are typically greater than for most hydrogels [16].

Many hydrogel fracture studies have considered mode III tearing tests [7] based on the classic analysis of Rivlin and Thomas [17] and allowing for direct comparisons with comparable tear tests in soft biological tissues [14, 18, 19]. However, there are challenges associated with gripping soft hydrogels in tension, and this approach does not easily allow for the high-throughput measurements associated with quantification of fracture stochastic behavior. For this reason, the approach here was adopted from the brittle particle fracture mechanics literature, in which tensile failure is induced in a sample via diametral compression [20, 21]. Spherical hydrogels of polyacrylamide and potassium polyacrylate were hydrated and compressed as a function of loading rate to measure the rate dependence and failure strength distribution.

Results

Hydrogel swelling and deswelling

As-received hydrogel spheres had a mass $m_0 = 23 \pm 3$ mg and diameter $d_0 = 3.1 \pm 0.05$ mm. Swollen spheres had a mass $m_s = 3030 \pm 284$ mg and diameter $d_s = 17.5 \pm 0.5$ mm. This corresponds to a mass swelling ratio $m_s/m_0 = 131.3$ and a volume swelling ratio $V_s/V_0 = 183.5$ (assuming spherical particles in volume calculations). The hydrogel beads reached equilibrium mass swelling in distilled water (DI) water in approximately 24 h [Fig. 1(a)], although they were not mechanically tested until at least 72 h (and typically 168 h) after the time of initial hydration. Fully hydrated beads lost less than 10% of their water mass in 100 min in ambient laboratory conditions [Fig. 1(b)] but were exposed to air for no more than 20 min for the slowest fracture tests and 60 min for the longest load relaxation tests. The swelling and deswelling profiles were consistent with the previously published work for similar gel spheres [22]. Every individual test, load relaxation or failure, was conducted with a different, fully hydrated sphere ($n = 212$ spheres total).

Load relaxation behavior

A small group of specimens was tested for short term ($n = 18$, Fig. 2) and long term ($n = 6$, Fig. 3) load relaxation behavior, where data are plotted for both the raw load–time response $P(t)$ and for the response normalized by the peak load P_0. In 60 s tests (Fig. 2), there was effectively no load relaxation over the test duration, and no strain level dependence, as shown by the collapse of normalized data onto the same approximate response. In hour tests (Fig. 3), there was some load relaxation over the duration of the test, but given the comparable relative mass loss for the particles sitting in ambient conditions for the same time frame as these long relaxation tests [Fig. 1(b)], it is likely that there was minimal load relaxation in the polymer network and the observed load decreases were at least partially due to deswelling. There was more variability in the long-time tests, but the normalized data again did not show a systematic trend with displacement level.

Failure properties

Representative load–displacement responses for the three displacement rates (1, 0.1, and 0.01 mm/s) are shown in Fig. 4(a), illustrating a nonlinear stiffening response and relatively little rate dependence in the load–displacement data. A representative hydrogel bead is shown in the undeformed and deformed near-failure state in Figs. 4(b) and 4(c), respectively, and in the video included in supplemental information. A representative failed specimen is shown in Fig. 4(d), illustrating brittle failure and fragmentation of the hydrogel bead into many small pieces.

The average and standard deviations for peak load, calculated peak stress, calculated effective elastic modulus, and calculated work to failure are show in Figs. 5(a)–5(d) as a function of testing displacement rate, where specimen numbers for failure tests were $n = 111$ for 1 mm/s, $n = 54$ for 0.1 mm/s, and $n = 25$ for 0.01 mm/s. Each parameter on average increased in proportion with increasing displacement rate.

Strength distributions

The empirical distribution functions for peak load and peak stress [23] are both shown in Fig. 6. When the peak stress data in Fig. 6(b) are pooled across displacement rates and plotted together in Fig. 7, it is clear that the data fall on a single empirical distribution for strength regardless of rate.

Discussion

The approach used here allowed for testing a large number of spherical hydrogel samples in compression as a function of loading rate, giving insight into their fracture behavior in an indirect but high-throughput manner; testing spheres in compression does not require sample gripping as in tensile testing, and thus allows for a quicker transition between mechanical experiments. Although average values of the peak force (measured) and peak stress, work of fracture, and elastic modulus (all calculated) did systematically increase with the loading rate (Fig. 5), the peak force or peak stress data all fell on a single curve (Fig. 7) regardless of the loading rate. There was overlap between the three different loading rates, with small strength values occurring at all three rates; the largest failure stresses were, however, uniformly seen at the fastest rate (Fig. 7). There have been interesting observations about the rate effects of fracture in rubbers and hydrogels in previous, tensile mode III studies. For example, in rubber, tensile elastic modulus showed no displacement rate dependence and samples exhibited very little load relaxation, but substantial displacement rate dependence in tear toughness [14]. The subject of decoupling intrinsic material time dependence from rate dependence observed in fracture of viscoelastic or poroelastic materials is a potential subject of significant future study within the field of hydrogels.

The geometry of a sphere compressed by two flat compression platens is consistent with Hertzian contact [24] at two points in the small strain elastic limit. This is consistent with the observed behavior from hydrogel spheres in the current study, as shown in Fig. 8, where the raw load–displacement data from Fig. 4(a) are replotted on log–log axes to enable easy observations of functional form of the load–displacement behavior along with illustrative lines representing different P–δ^m relationships. The $P \propto \delta^{3/2}$ Hertzian relationship [24] is apparent at small displacements, that is, for the first 1–2 mm of displacement. At larger displacements, there is a transition to a substantially stiffer behavior, approaching $P \propto \delta^5$ immediately before failure (Fig. 8). This stiffening is consistent with the behavior observed in similar experiments with rubber spheres

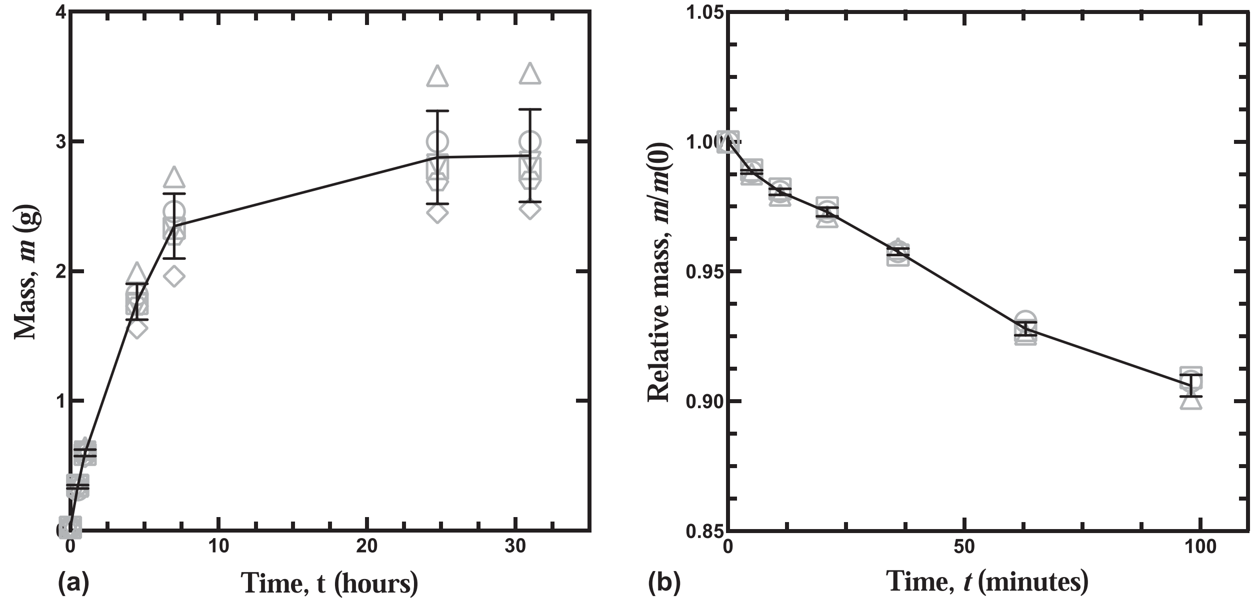

Figure 1: (a) Hydrogel bead mass swelling in DI water (n = 6) and (b) hydrogel bead deswelling in air over the experimental time frame (n = 3).

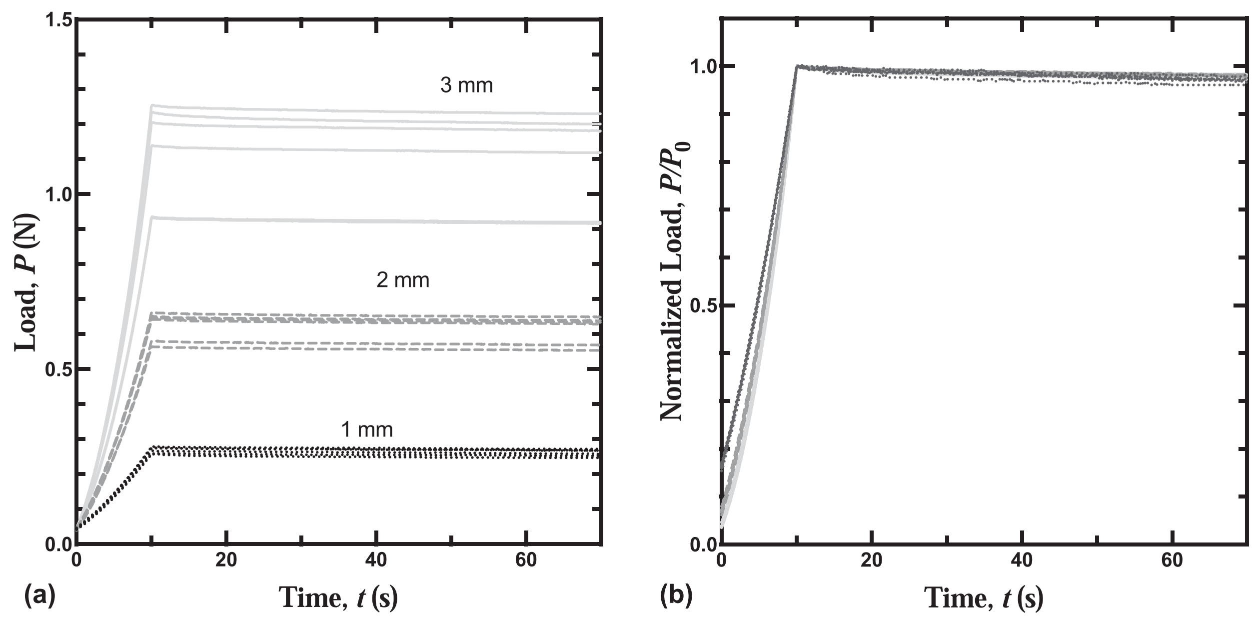

Figure 2: (a) Hydrogel bead raw load relaxation for three different displacement levels δ = 1, 2, and 3 mm (n = 6 for each) for 60 s of relaxation and (b) normalized relaxation data from (a) demonstrating nearly elastic responses over 60 s for all three displacement levels.

[25, 26, 27, 28] in which a $P \propto \delta^3$ to $P \propto \delta^5$ relationship has been observed for large deformations. Tatara and colleagues treat the rubber particles they compress as neo-Hookean and differentiate between an initial, zero-strain elastic modulus E_0 and a finite-strain elastic modulus E dependent on the strain. However, their work does not calculate the strain-dependent elastic modulus as it focusses on the load–displacement behavior and shape of the deformed particles. As such, here a Hertzian approximation was used to calculate E_{eff} [Fig. 5(c)] acknowledging that because this is from the peak point (P_{max} and δ_{max}), it is an overestimate of the zero-strain value E_0. The size of this overestimate can be approximated from calculating E based on the force $P \sim 0.1$ N at $\delta = 1$ mm displacement for all loading rates in Fig. 8, this gives E of 54 kPa compared with the mean values in the hundreds of kPa in Fig. 5. However, this approximation was chosen to isolate the effects of the loading rate on E_{eff} because the greatest differentiation between the load–displacement curves in this study was at the peak point.

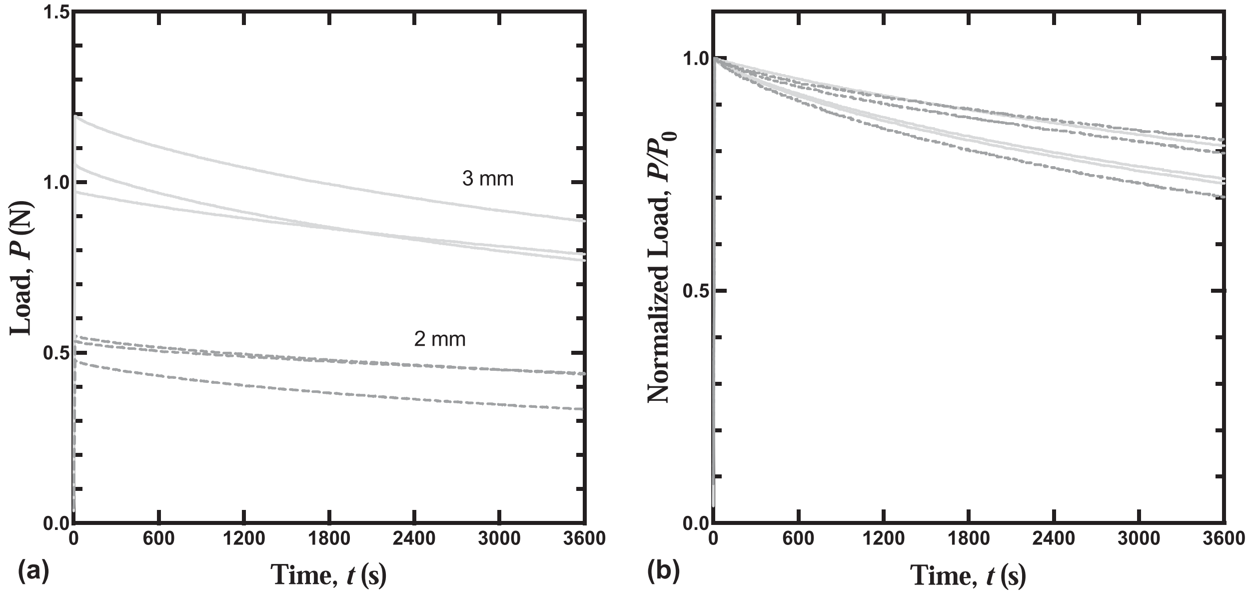

Figure 3: (a) Hydrogel bead raw load relaxation for two different displacement levels $\delta = 2$ and 3 mm ($n = 3$ for each) for one hour of relaxation and (b) normalized relaxation data from (a) demonstrating on average an 11% decrease in peak force at 1200 s and a 20–30% decrease in peak force over the course of one hour. This relaxation is likely due largely to deswelling over the relaxation time frame.

Future studies will aim to implement the neo-Hookean model in numerical simulations to allow for the full characterization of E as a function of strain, but this was beyond the scope of the current work focusing on failure behavior.

There is an extensive literature on the compression fracture of brittle particles, such as glass and plaster. In these studies, different empirical expressions have been used to calculate the maximum stress in the form of [21]

$$\sigma = f\frac{P}{\pi r^2} \quad , \tag{1}$$

where f is a prefactor, sometimes expressed as $f(\nu)$, a function of Poisson's ratio, of order one. Frequently, this prefactor is reported to be smaller than one, sometimes larger than one, and often around 0.8. Because of the wide range of reported values for this prefactor in different studies (reviewed in Ref. 21), f here was taken as unity and the characteristic stress here was simply calculated as $P/\pi r^2$. In comparing the fracture morphologies of the fragments found in the current study, the hydrogel fragments were smaller and of less distinct shape than those reported for glass, ceramic, or plaster particles [29, 30], which are sometimes referred to as "orange segment" shaped. Brittle ceramics failed by chipping or division into several large pieces far more often [29] than the fragmentation observed in the current study with brittle hydrogels.

The tests performed in the current study were executed in ambient laboratory conditions, as the test frame being used for testing was not set up with a water bath for testing in immersed conditions. The potential effect of deswelling of the hydrogels was assessed by the weight experiment presented in Fig. 1(b) and in the long-term load relaxation tests reported in Fig. 3. Interestingly, this effect did not seem to dramatically affect the fracture data because the results all fell on the same curve (Fig. 7) and peak stress values for the fastest loading rate overlapped with those of the slowest rate. Future studies will endeavor to address this limitation by establishing a mechanism for locally hydrating the samples, perhaps with an atomizer to spray the gels with fluid during the tests.

This study was undertaken with commercially sourced hydrogels that were spherical and sold in the dehydrated state. The material system was polyacrylamide–potassium polyacrylate, both of which are very common commercial hydrogels. Polyacrylamide is frequently one of two polymers used in double-network gel studies, for example, with alginate [8], and it has been the subject of extensive mechanical studies [31]. Potassium polyacrylate is a superabsorbent and charged component frequently used in domestic products, such as diapers, and the combination of the two gels is commonly used in agricultural applications [32]. Future studies using the methods used here will require designing a method to create hydrogel spheres in other chemistries. However, the current system presents opportunities for further studies on the effects of solvent because the charged component of the gel can be manipulated with changing salt concentration.

Conclusions

This study presented a method and results for testing of hydrogel failure in a high-throughput manner using the spherical particle diametral compression test, as studied extensively in the brittle material literature. Loading rate dependence

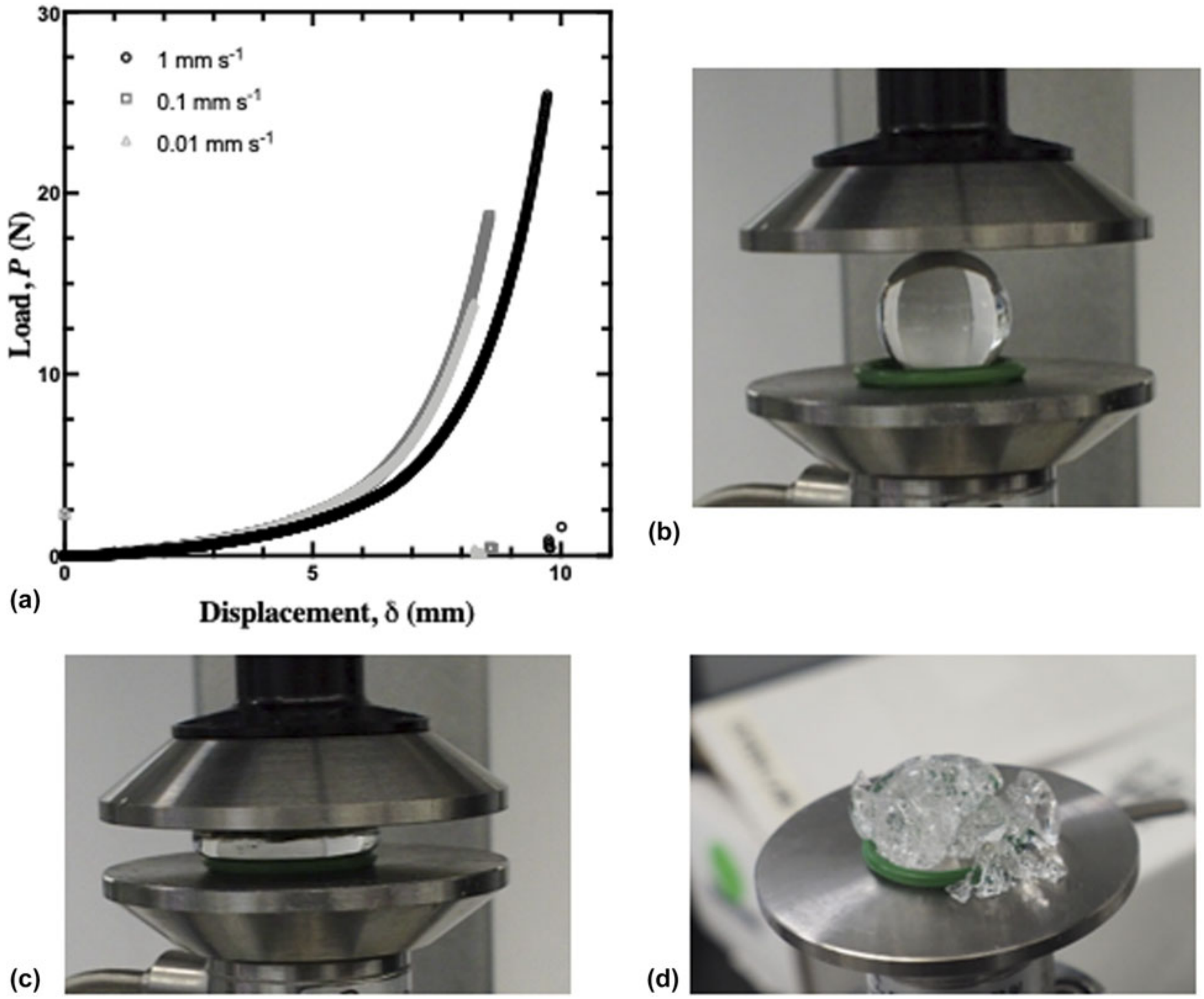

Figure 4: (a) Representative load–displacement (P–δ) curves for compression of hydrogel spheres at three rates $d\delta/dt$ = 1, 0.1, and 0.01 mm/s. Stiffening responses with increasing displacement are illustrated, as is the catastrophic nature of failure with force dropping to near zero in one time increment. The sphere shown (b) before deformation and (c) near peak deformation before failure, which occurred at approximately 50% nominal grip strain, and (d) after failure.

in fracture load was observed, but the overall distribution of fracture stresses was a smooth curve ranging from 0.05 to 0.3 MPa for polyacrylamide–potassium polyacrylate swollen in distilled water.

Materials and methods

Hydrogel sphere preparation

Translucent polymer spheres of polyacrylamide–potassium polyacrylate were commercially sourced (Carolina Biological Supply Company), hydrated, and tested for time-dependent load relaxation and failure properties. For each polymer sphere, an original mass and diameter were recorded. Sterile 50 mL Falcon tubes were then filled with 25 mL of distilled water and a single polymer sphere per tube. These spheres were left stationary at room temperature for seven days to ensure swelling had equilibrated. After the seven days, water was drained from the Falcon tube leaving only the swollen polymer sphere. The final mass (measured with a balance) and diameter (measured with calipers) were taken for each swollen polymer sphere, and mass and volume swelling ratios were calculated.

Mechanical testing

All mechanical tests were performed with a TA Instruments 5500 Series ElectroForce universal test frame using WinTest software. The power supply and ElectroForce instrument were turned on 30 min before testing to ensure accurate data collection, per recommendations from the manufacturer. ElectroForce was equipped with a 50 lbf load cell and a set of compression platens. A ramp test was used and configured for the upper platen to move downward 10 mm at displacement

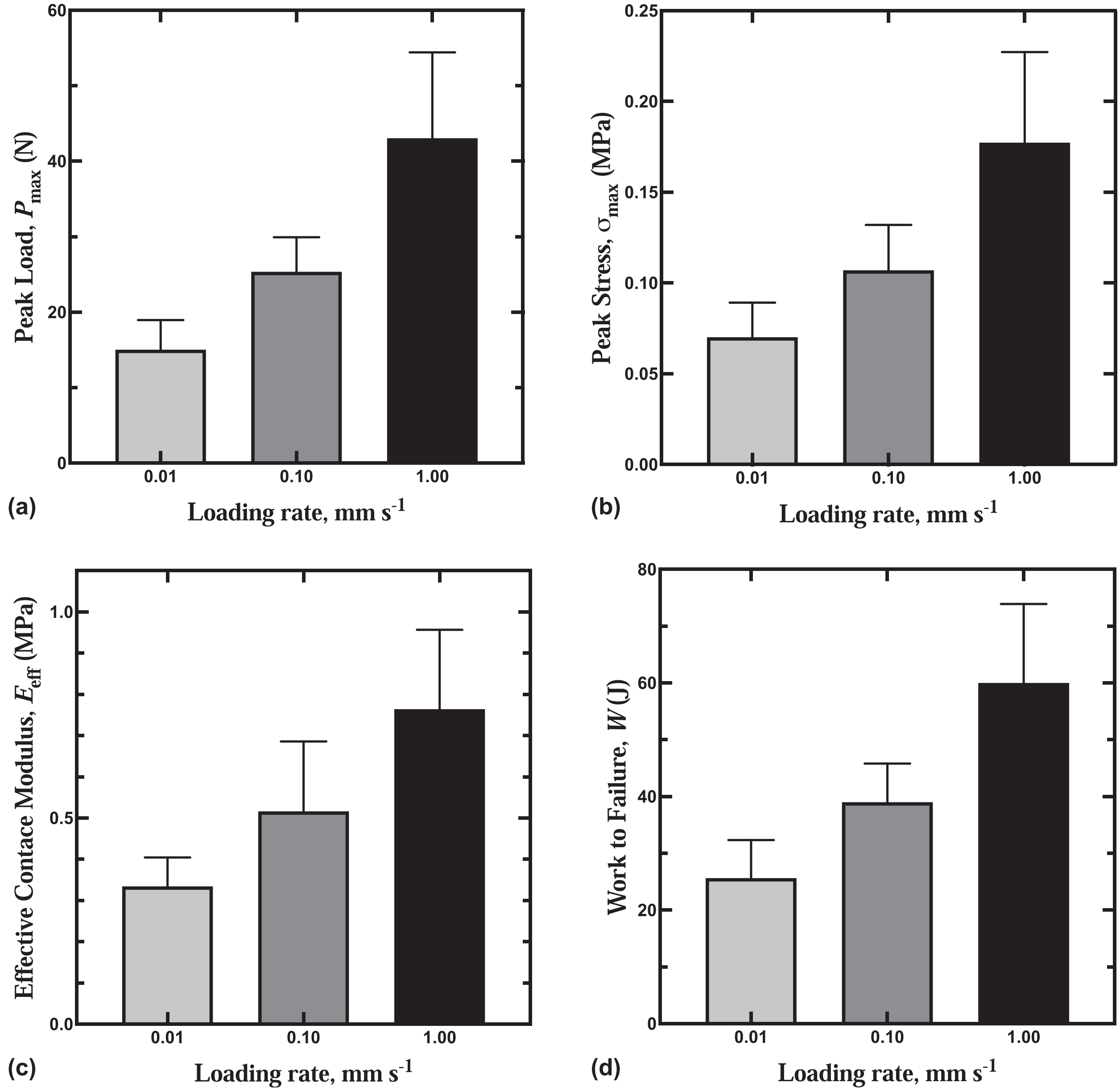

Figure 5: Average properties as a function of compressive loading rate for hydrogel spheres showing (a) peak load P_{max}, (b) peak stress σ_{max} calculated from P_{max} and sphere diameter d, (c) effective contact modulus E_{eff} calculated assuming Hertzian mechanics, and (d) work to failure W from numerical integration of the load–displacement data to the point of load drop. All properties increased slightly with faster loading rates.

rates of 1, 0.1, and 0.01 mm/s. A rubber O-ring was placed around the polymer sphere on the lower platen to prevent the sphere from sliding out. Once the polymer sphere was moved to be slightly out of contact from the upper platen, and the load cell was zeroed the ramp test began. Data acquisition was set up to collect 1000 data points for each test, changing acquisition rate with displacement rate.

Analytical methods

The raw data for each trial consist of time t (s), load P (N), and displacement δ (mm). The data collected were analyzed using spreadsheet software (MS Excel; Microsoft, Redmond, WA), and for each specimen, the peak load P_{max} (N), and associated peak stress σ_{max} (MPa), Young's modulus E (MPa), and work to failure W (J) were calculated as follows. The peak load was defined to be the maximum load on the specimen before fracture, the first load drop (manually noted and which in this study was typically a catastrophic specimen failure). A characteristic peak engineering stress or strength, σ_{max}, was found by dividing the peak load P_{max} by the area of a circle defined by the swollen diameter d_s of each sphere, $\sigma_{max} = P_{max}/\pi(d_s/2)^2$.

Journal of Materials Research ■ Volume 35 ■ Issue 10 ■ May 28, 2020 ■ www.mrs.org/jmr

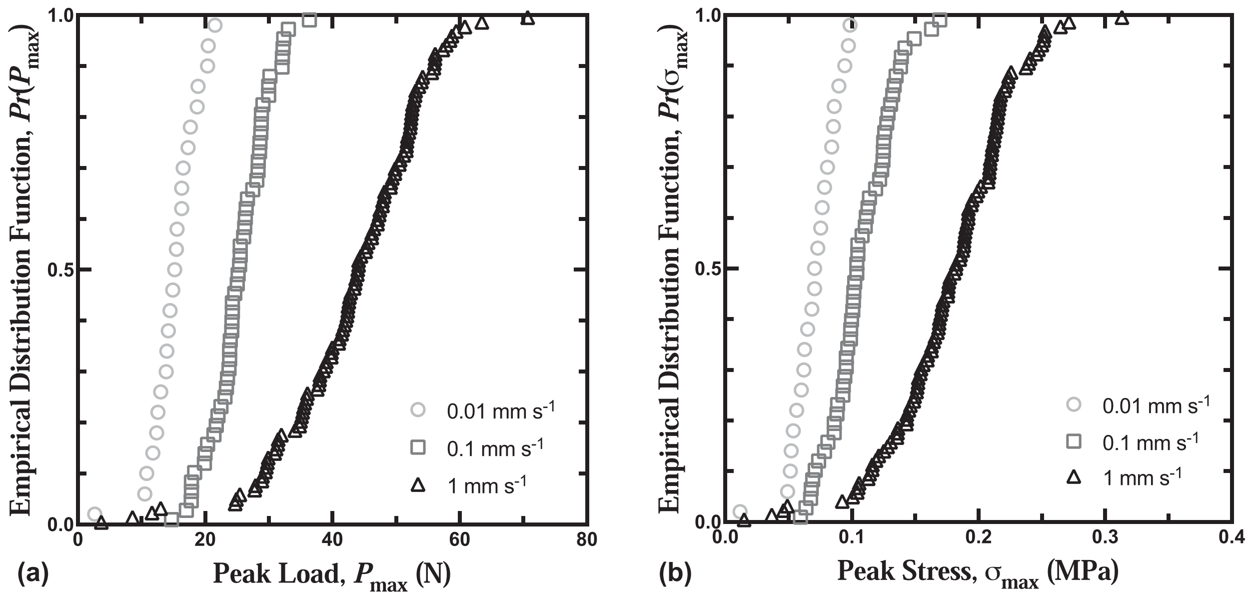

Figure 6: Empirical distribution functions Pr(x) versus x for (a) peak load P_{max} and (b) peak stress σ_{max} as a function of displacement rate. Specimen numbers for failure tests were n = 111 for 1 mm/s, n = 54 for 0.1 mm/s, and n = 25 for 0.01 mm/s.

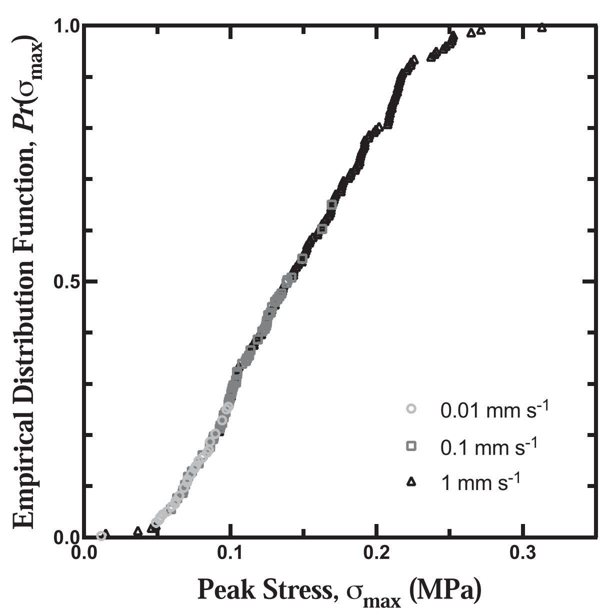

Figure 7: Empirical distribution function Pr(x) versus x for peak stress σ_{max} for all data from Fig. 6(b) pooled and ordered regardless of displacement rate. The data fall on a single curve that is sigmoidal with a large midrange of nearly linear behavior.

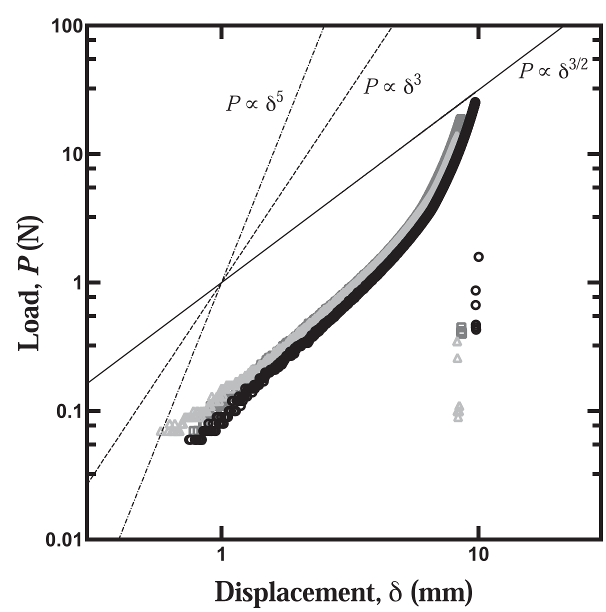

Figure 8: Load–displacement (P–δ) data from Fig. 4(a) replotted on a log–log scale using the same symbols, illustrating the transition from Hertzian behavior ($P \propto \delta^{3/2}$) at small displacements to approximately $P \propto \delta^5$ at large displacements.

Using Hertzian contact [24], the effective contact modulus E_{eff} was calculated from the peak load P_{max} and displacement at peak load δ (P_{max}) by rearranging

$$P = 4/3\, R^{1/2} E^{*} h^{3/2} \quad , \tag{2}$$

where $h = \delta/2$ because there are two points of Hertzian contact at the contacts between the sphere and each compression platen, $R = d_s/2$ the swollen sphere radius, and $E^* = E_{eff}/(1 - \nu^2)$ where Poisson's ratio ν has been assumed to be 0.5. To calculate the work to failure W, a definite integral was used, finding the area under the force–displacement curve by fitting the force–displacement data to a fifth-order polynomial and calculating the integral from zero up to the failure (load drop) point.

To calculate the empirical distribution functions for failure, Pr(x) versus x, the data values x (P_{max} or σ_{max}) were

Journal of Materials Research ■ Volume 35 ■ Issue 10 ■ May 28, 2020 ■ www.mrs.org/jmr

ordered from smallest to largest and assigned a rank index i for $n = i_{\max}$ total values per grouping. Plots were then generated for $\Pr(x) = (i - 0.5)/i_{\max}$. and plotted versus $x = P_{\max}$ or $\sigma_{\max}$ [23].

Acknowledgments

The authors acknowledge the critical contributions of Dana Al Jalal and Leena Dakhaikh, students from IAU, Saudi Arabia, who were visiting researchers at ECU in the Summer 2019 and who helped with the experiments and data analysis. Funding was provided by the ECU Division of Research, Economic Development and Engagement (REDE) via start-up funds to MLO. JDJ was funded during part of this study via an REU studentship, Biomedical Engineering in Simulations, Imaging, and Modeling (BME-SIM), Award #1359183, from the National Science Foundation.

Supplementary material

To view supplementary material for this article, please visit https://doi.org/10.1557/jmr.2020.114.

References

1. **J.L. Drury and D.J. Mooney**: Hydrogels for tissue engineering: Scaffold design variables and applications. *Biomaterials* **24**, 4337 (2003).
2. **A.M.S. Costa and J.F. Mano**: Extremely strong and tough hydrogels as prospective candidates for tissue repair—A review. *Eur. Polym. J.* **72**, 344 (2015).
3. **J. Li, E. Weber, S. Guth-Gundel, M. Schuleit, A. Kuttler, C. Halleux, N. Accart, A. Doelemeyer, A. Basler, B. Tigani, K. Wuersch, M. Fornaro, M. Kneissel, A. Stafford, B.R. Freedman, and D.J. Mooney**: Tough composite hydrogels with high loading and local release of biological drugs. *Adv. Healthcare Mater.* **7**, 1701393 (2018).
4. **T.R. Hoare and D.S. Kohane**: Hydrogels in drug delivery: Progress and challenges. *Polymer* **49**, 1993 (2008).
5. **K. Varaprasad, G.M. Raghavendra, T. Jayaramudu, M.M. Yallapu, and R. Sadiku**: A mini review on hydrogels classification and recent developments in miscellaneous applications. *Mater. Sci. Eng., C* **79**, 958 (2017).
6. **M.L. Oyen**: Mechanical characterization of hydrogel materials. *Int. Mater. Rev.* **59**, 44 (2014).
7. **J.P. Gong**: Why are double network hydrogels so tough? *Soft Matter* **6**, 2583 (2010).
8. **J-Y. Sun, X. Zhao, W.R. Illeperuma, O. Chaudhuri, K.H. Oh, D.J. Mooney, J.J. Vlassak, and Z. Suo**: Highly stretchable and tough hydrogels. *Nature* **489**, 133–136 (2012).
9. **F-m. Cheng, H-x. Chen, and H-d. Li**: Recent advances in tough and self-healing nanocomposite hydrogels for shape morphing and soft actuators. *Eur. Polym. J.* **124**, 109448 (2020).
10. **K. Tonsomboon and M.L. Oyen**: Composite electrospun gelatin fiber-alginate gel scaffolds for mechanically robust tissue engineered cornea. *J. Mech. Behav. Biomed. Mater.* **21**, 185 (2013).
11. **A.L. Butcher, G.S. Offeddu, and M.L. Oyen**: Nanofibrous hydrogel composites as mechanically robust tissue engineering scaffolds. *Trends Biotechnol.* **32**, 564 (2014).
12. **G.S. Offeddu, I. Mela, P. Jeggle, R.M. Henderson, S.K. Smoukov, and M.L. Oyen**: Cartilage-like electrostatic stiffening of responsive cryogel scaffolds. *Sci. Rep.* **7**, 42948 (2017).
13. **Y. Xiao, D.A. Rennerfeldt, E.A. Friis, S.H. Gehrke, and M.S. Detamore**: Evaluation of apparent fracture toughness of articular cartilage and hydrogels. *J. Tissue Eng. Regener. Med.* **11**, 121 (2017).
14. **K. Tonsomboon, C-T. Koh, and M. Oyen**: Time-dependent fracture toughness of cornea. *J. Mech. Behav. Biomed. Mater.* **34**, 116 (2014).
15. **C. Creton and M. Ciccotti**: Fracture and adhesion of soft materials: A review. *Rep. Prog. Phys.* **79**, 046601 (2016).
16. **K. Tonsomboon, A.L. Butcher, and M.L. Oyen**: Strong and tough nanofibrous hydrogel composites based on biomimetic principles. *Mater. Sci. Eng., C* **72**, 220 (2017).
17. **R.S. Rivlin and A.G. Thomas**: Rupture of rubber. I. Characteristic energy for tearing. *J. Polym. Sci.* **10**, 291 (1953).
18. **M.V. Chin-Purcell and J.L. Lewis**: Fracture of articular cartilage. *J. Biomech. Eng.* **118**, 545 (1996).
19. **P.P. Purslow**: Positional variations in fracture toughness, stiffness, and strength of descending thoracic pig aorta. *J. Biomech.* **16**, 947 (1983).
20. **J.C. Jaeger**: Failure of rocks under tensile conditions. *Int. J. Rock Mech. Min. Sci.* **4**, 219 (1967).
21. **B.W. Darvell**: Uniaxial compression tests and the validity of indirect tensile strength. *J. Mater. Sci.* **25**, 757 (1990).
22. **T. Bertrand, J. Peixinho, S. Mukhopadhyay, and C.W. MacMinn**: Dynamics of swelling and drying in a spherical gel. *Phys. Rev. Appl.* **6**, 064010 (2016).
23. **Y. Rozenblat, D. Portnikov, A. Levy, H. Kalman, S. Aman, and J. Tomas**: Strength distribution of particles under compression. *Powder Technol.* **208**, 215 (2011).
24. **K.L. Johnson**: *Contact Mechanics* (Cambridge University Press, U.K., 1985).
25. **Y. Tatara, S. Shima, and J.C. Lucero**: On compression of rubber elastic sphere over a large range of displacements—Part 1: Theoretical study. *J. Eng. Mater. Technol.* **113**, 285 (1991).
26. **Y. Tatara**: On compression of rubber elastic sphere over a large range of displacements—Part 2: Comparison of theory and experiment. *J. Eng. Mater. Technol.* **113**, 292 (1991).
27. **Y. Tatara**: Large deformations of a rubber sphere under diametrical compression (Part I: Theoretical analysis of press approach, contact radius, and lateral extension). *JSME Int. J. Ser. A, Mech. material Eng.* **36**, 190 (1993).
28. **S. Shima, Y. Tatara, M. Iio, C. Shu, and J.C. Lucero**: Large deformations of a rubber sphere under diametral compression (Part 2: Experiments on many rubber materials and comparisons

of theories with experiments). *JSME Int. J. Ser. A, Mech. material Eng.* **36**, 197 (1993).

29. **M.A. Verspui, G. de With, and E.C.A. Dekkers**: A crusher for single particle testing. *Rev. Sci. Instrum.* **68**, 1553 (1997).
30. **T. Chen, Q. Fang, Z. Wang, and W. Zhu**: Numerical simulation of compression breakage of spherical particle. *Chem. Eng. Sci.* **173**, 443 (2017).
31. **C. Yang, T. Yin, and Z. Suo**: Polyacrylamide hydrogels I: Network imperfection. *J. Mech. Phys. Solid.* **131**, 43 (2019).
32. **H.A. Abd El-Rehim, E.A. Hegazy, and H.L. Abd El-Mohdy**: Effect of various environmental conditions on the swelling property of PAAm/PAAcK superabsorbent hydrogel prepared by ionizing radiation. *J. Appl. Polym. Sci.* **101**, 3955 (2006).